VLA Scientific Memo. No. 177

Some Issues for Water Vapor Radiometry at the VLA

Bryan Butler
National Radio Astronomy Observatory

December 6, 1999

Introduction

As part of the VLA Upgrade Project (Bastian & Bridle 1994), new low-noise, high-efficiency K-band (18-26 GHz) receiver systems are being constructed and placed on the antennas of the VLA. Water vapor radiometry (WVR) systems have been designed to be placed alongside these new receivers. These WVR systems are similar to Dave Woody's in design (Marvel & Woody 1998), with modifications. This memo will attempt to describe these WVR systems in general terms and to describe some possible design considerations and problems for these systems.

Overview

Phase fluctuations introduced as radio waves pass through the Earth's atmosphere are a fundamental limitation to the ability to do high quality interferometry. These phase fluctuations limit the achievable dynamic range, fidelity, and resolution of interferometer arrays. There is a very long history of discussion of this topic, so I will not dwell on details here (see e.g., Welch [1999] for a very good discussion of the history of this topic). Because of the evils of atmospherically induced phase fluctuations, it is desirable to devise a method for tracking and correcting for them. These fluctuations are caused almost entirely (at radio wavelengths) by fluctuations in atmospheric water vapor. Because atmospheric water vapor also serves as an emission source, a natural method to pursue for phase fluctuation correction is that of radiometry, i.e., measuring the fluctuations in emission temperature (sky brightness) and using those to infer a fluctuation in the amount of water vapor and hence in the phase. These techniques have been pursued at some level for over 30 years now (again, see Welch [1999]), and are fairly well developed. There is a large amount of literature on the subject, so I will not expound (for relatively recent discussion see e.g., Carilli & Holdaway 1999; Lay 1997; Wright 1996; Sutton & Hueckstaedt 1996).

There are two fundamental types of water vapor radiometry useful in this respect - *continuum* and *line*. In continuum radiometry, a contiguous chunk of frequency space (e.g., near 230 GHz) is monitored for absolute fluctuations in emission. This type of radiometric system has been shown to be successful for correcting atmospheric phase fluctuations, and is in fact used regularly at the IRAM millimeter interferometer (see e.g., Bremer *et al.* 1996). However, it is well known that this type of system fails in the presence of liquid water (e.g. clouds or fog). Liquid water is a particular annoyance for all types of radiometry which are concerned with correcting for phase fluctuations, because liquid water is a bright emission source but does little to the phase. In line radiometry, measurements of one of the emission lines of atmospheric water are made at several frequencies, and these are used to determine the fluctuations in the atmospheric water. In principle, such systems can distinguish between water vapor and liquid, due to different spectral shapes of the two types of emission. For such systems, a decision must be made on which emission line to attempt to measure (e.g. 22 or 183 GHz). Systems utilizing measurements of either of these water lines have been shown to work at least under some conditions (see e.g. Marvel & Woody 1996; Lay *et al.* 1998; Wiedner 1998).

There is a relatively long history of WVR at NRAO (see e.g., Waters 1967; Waters 1971), and some history with WVR systems at the VLA (Resch *et al.* 1984), but the sensitivity and stability of these systems was not good enough to make them particularly attractive. Only with recent developments in this area has it seemingly become possible to put such systems to good use on the VLA antennas. Therefore, the decision was made several years ago to attempt to do WVR once again at the VLA. Initial work concentrated on using the present system temperature monitoring system to do the WVR (Bagri 1994). Of course, being effectively a single channel system, and with relatively coarse resolution, it was rather quickly decided that such a system would not work well (again, liquid water is a problem). At about this same time, the program to replace the current K-band (near 22 GHz) receivers on the VLA antennas was starting to develop. The receiver replacement would result in an improvement in system temperature of nearly a factor of 3. Since the receivers were being redesigned, it was decided that a WVR system should be designed in to the new receivers from the start (Bagri 1995). Given the failure of the single channel systems in the presence of cloud, and the fact that the VLA site often has clouds above it, it was clear that a line system was preferred to a single channel system. The fact that the system would be part of the K-band receiver system necessarily implied that the 22 GHz line would be the one monitored. In fact, this is the right decision, since the amount of atmospheric water vapor above the VLA site (in summer months, at least) causes the 183 GHz line to saturate through a wide frequency range about its center. Because of electronics considerations, and prompted by the success of the OVRO system, it was decided that a 3-channel system would be designed and tested initially as the WVR system attached to the upgrade K-band receivers for the VLA.

Current VLA WVR design

A simplified block diagram for the current VLA WVR design is shown in Figure 1. For more details and specific components, see Watts (1999). After reception through the feed horn, the signal is split into right and left polarizations. Currently only one polarization has a WVR attached to it (LCP). After polarization selection, the noise cal injection occurs (at 9.6 Hz). The signal is then amplified (cooled), filtered (18-26 GHz), and amplified (room temp) again. At this point, the signal goes through a 2-way splitter, with one path leading to the LO injection point and hence to the radio astronomy system, and the other path leading to the WVR system.

The WVR system takes the signal through an initial bandpass filter of 20.5-24 GHz. This bandpass filter was not part of the initial design, but it was discovered that without it, LO signal leaked into the WVR system and corrupted the signal. So, this filter was added, and the bandwidths and central locations of the 3 final bandpass filters were adjusted to accomodate this new arrangement. After passing through this initial bandpass filter, the signal then goes through another amplifier stage, and into a 4-way splitter. From the 4-way splitter, the signal goes through one of 3 final bandpass filters (to be discussed in detail later), is detected with a tunnel diode detector, and A/D is performed with a voltage to frequency converter. At this point, the digitized signal values are interfaced into the monitor and control system, where they are passed with other M&C data along the waveguide to the control building, after accumulation. The on-line system is presented with 6 values every 5/6 second - the values for the 3 filter channels both for noise-cal on and noise-cal off. When the noise-cal is off, the detected voltage (V_{off}) is proportional to the total system temperature T_{sys}. When the noise-cal is on, the detected voltage (V_{on}) is proportional to the sum of the system temperature and the equivalent noise-cal temperature T_{cal}. So, the system temperature for each filter channel can be formed via:

$$T_{sys} = G\, T_{cal}\, \frac{V_{off}}{V_{on} - V_{off}} \quad , \tag{1}$$

where G is the system gain factor.

Given this formulation for the system temperature, the rms on the measurement is:

$$\frac{\sigma_{T_{sys}}}{T_{sys}} = \sqrt{\left(\frac{\Delta G}{G}\right)^2 + \left(\frac{\Delta T_{cal}}{T_{cal}}\right)^2 + \frac{2}{B\tau}\left[1 + \frac{(T_{sys} + T_{cal})^2 + T_{sys}^2}{T_{cal}^2}\right]} \quad , \tag{2}$$

where $\Delta G/G$ is the gain fluctuation in the detection system, ΔT_{cal} is the fluctuation in the equivalent noise-cal temperature, B is the bandwidth, and τ is the integration time. If we assume that $T_{sys} \gg T_{cal}$, the above simplifies to:

$$\frac{\sigma_{T_{sys}}}{T_{sys}} = \sqrt{\left(\frac{\Delta G}{G}\right)^2 + \left(\frac{\Delta T_{cal}}{T_{cal}}\right)^2 + \frac{4}{B\tau}\,\frac{T_{sys}^2}{T_{cal}^2}} \quad . \tag{3}$$

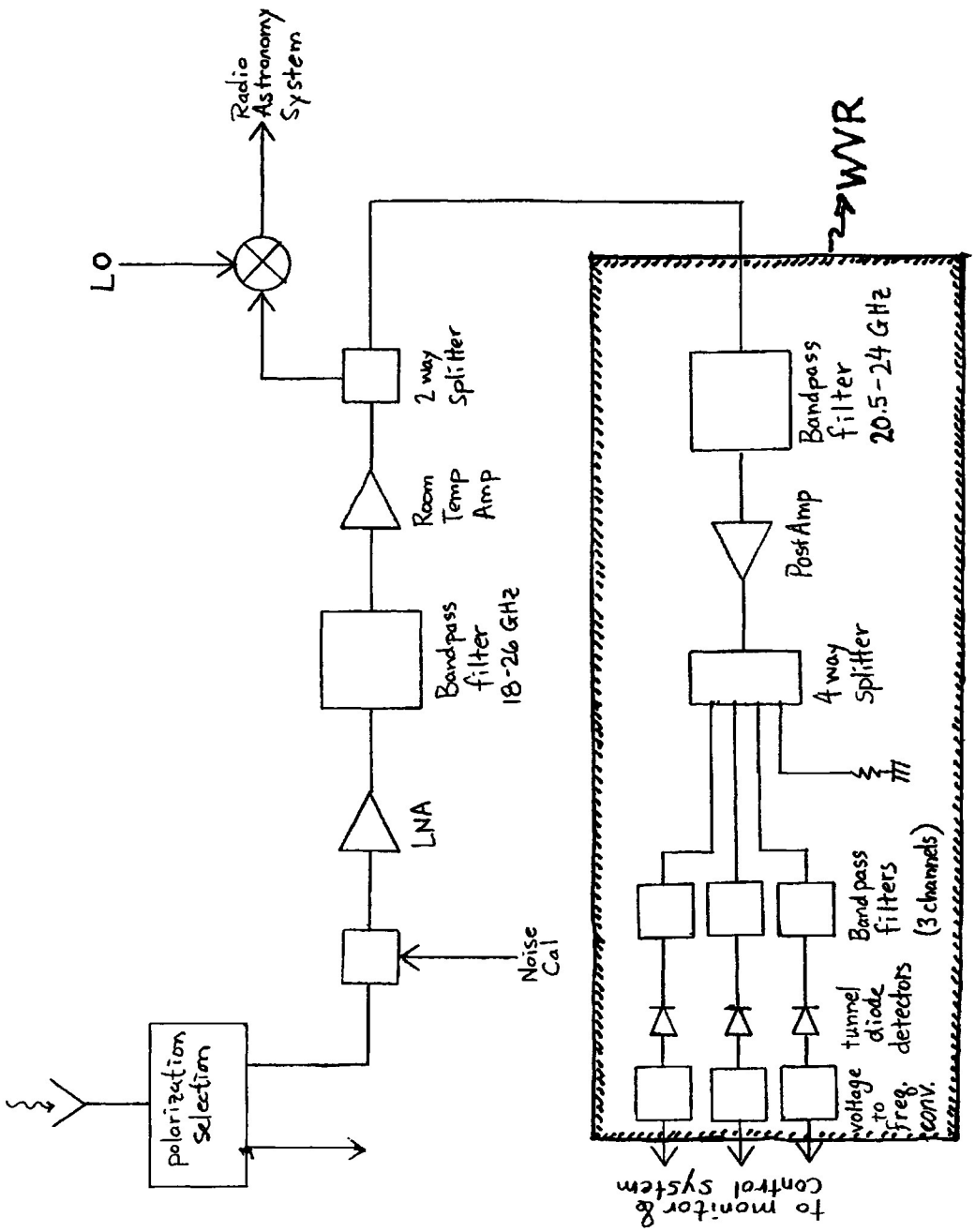

Figure 1: Simplified block diagram of current VLA WVR system.

Making the further assumption that the gain and noise-cal fluctuations are negligibly small it further simplifies to:

$$\frac{\sigma_{T_{sys}}}{T_{sys}} \sim \frac{2}{\sqrt{B\,\tau}} \frac{T_{sys}}{T_{cal}} \quad . \tag{4}$$

Let us examine the magnitude of this rms for the upgrade K-band systems on the VLA. The value of T_{sys} is roughly 50 to 100 K at zenith, depending on atmospheric opacity (3% at the very best, 25% when bad). The value of T_{cal} is of order 5 K. So, for a 1 GHz bandwidth and 1 second integration time, the rms is of order 30 to 120 mK. Decreasing the bandwidth to 300 MHz causes the rms to increase to of order 60 to 240 mK. Remember that these are lower limits, since they assume that there are no gain or noise-cal fluctuations in the detection system.

There are three more things to note here. The first is that the type of radiometer system being employed here is less sensitive than a traditional Dicke switched system. A Dicke switched system with our range of antenna (essentially atmospheric) temperatures and receiver temperatures would have an rms of the order of a few to 10 mK at $B = 1$ GHz (to first order, the difference is that the Dicke switched system would not have the T_{sys}/T_{cal} term so it would be an order of magnitude more sensitive). The second is that the quantity that we *really* want is the atmospheric temperature, *not* the total system temperature T_{sys}. If we knew exactly what the effective receiver temperature (T_{Rx}) was, then this would be relatively unimportant, but the fact is that we do not monitor our receiver temperatures carefully. Now, we are saved in some sense by the fact that we have a multi-channel system, so that we can work with differences in the T_{sys} values for the channels and mostly cancel out the non-atmospheric contributions to T_{sys}. However, changes in receiver temperature and other contributors to T_{sys} (ground pickup, for instance) as a function of frequency (i.e., where the filters are placed) may become an important limitation in our current design. The third thing to note is that we don't really have good values for T_{cal} for our receiver systems. We also have no good information on their fluctuations.

Proposed goal of VLA WVR system

VLA "electronic" stability

Even given no atmosphere above the VLA antennas, phase errors would still exist in the observed visibilities. These are due to instrumental (true electronics), quantization, and residual baseline errors, among other things. These things are often referred to as the "electronic phase noise" even though they are not necessarily entirely electronic. For the VLA, this electronic phase noise is of order:

$$\Delta\phi_e \sim \frac{\nu_{GHz}}{4} \quad , \tag{5}$$

where $\Delta\phi_e$ is in degrees, and ν_{GHz} is the frequency in GHz (see e.g., Sramek 1989). This number is of interest because it makes no sense to make the WVR system capable of correcting atmospheric fluctuations to much better than this electronic phase fluctuation.

Relation between path length and phase

A blob of water vapor of extent Δh which intercepts the incoming radio waves in front of one antenna in an interferometer pair causes a phase difference of:

$$\Delta\phi \sim 360 \frac{6.3\ \Delta h}{\lambda} \quad , \tag{6}$$

where $\Delta\phi$ is in degrees and λ is the wavelength of observation. The factor of 6.3 converts from path length of water vapor to absolute path length, and is certainly an approximation (see the derivation in Waters 1967), but is good enough for definition of the goals of the WVR system. So, as an example, a water vapor excess of 175 μm would cause a phase difference of 1 radian at 7 mm wavelength.

Proposed goal

Again, it makes little sense to attempt to fix the atmospheric phase fluctuations to better than the electronic noise. If these two contributions to total phase fluctuation are set equal, this leaves:

$$\Delta\phi = \Delta\phi_e \qquad \Rightarrow \qquad \Delta h \sim \frac{c}{9.1 \times 10^{12}} \sim 35\,\mu\text{m} \quad . \tag{7}$$

Thus the ability to correct for fluctuations in water vapor as small as 35 μm should be the goal for the VLA WVR system. This corresponds to a total path length fluctuation of roughly 220 μm, a phase of 10° at 7 mm (43 GHz), or $\lambda/30$ at 7 mm.

Atmospheric model

In order to investigate the operation of the VLA WVR system, a model for atmospheric emission is necessary. In my treatment, this is broken into two basic parts: creation of model atmosphere; and calculation of emission from that atmosphere as a function of frequency.

Model atmosphere creation

The model atmosphere is defined by specifying the pressure, temperature, water vapor (either relative humidity or vapor pressure of water), and liquid water information for some arbitrary number of levels in the atmosphere. I have the ability to define the maximum height of the model atmosphere and the vertical distance between levels. Temperature as a function of altitude is calculated by specifying some surface temperature, then using sensible values of

the lapse rate ($\partial T/\partial z$) as a function of altitude. Pressure is calculated by specifying the altitude of the lowest level in the model atmosphere (the altitude of the VLA, in this specific case), and assuming an exponential pressure decrease with altitude. The scale height for the decrease is calculated as a function of altitude using the appropriate temperature. The vapor pressure of water is calculated by specifying some total precipitable water vapor, and assuming an exponential decay with altitude. In this case, a constant (specified) scale height for the decrease is used (generally this should be between 1.5 and 2 km). Care must be taken if saturation in any layer occurs. To account for this, if saturation occurs in any level, the vapor pressure of water is assigned to be the saturation vapor pressure (calculated with the formulation of Buck 1981), and the profile is recalculated (this is repeated until converged). Liquid water is specified as a cloud layer of given height and extent and liquid water content.

So, the necessary inputs for the model atmosphere creation are: altitude, latitude (used for calculating the surface gravity and height of tropopause), surface temperature, total precipitable water vapor, water vapor scale height, maximum altitude in the model, vertical distance between levels, and cloud parameters (height, extent, and liquid water content). Figure 2 shows a plot of temperature and water vapor pressure for such a model atmosphere for the VLA with the surface temperature set to 5° C, total precipitable water vapor of 7 mm, water vapor scale height of 2 km, maximum altitude of 30 km, distance between levels of 200 m, and no cloud. Note the saturation of water vapor near the tropopause (just above 10 km).

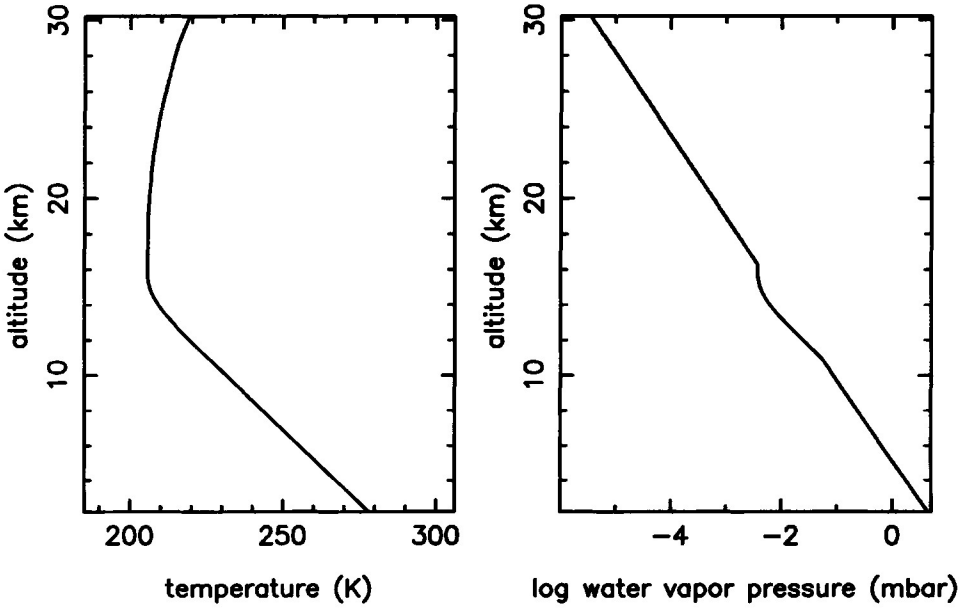

Figure 2: Temperature and water vapor pressure components of an example atmospheric model.

For all of the model runs discussed in this memo, a surface altitude of 2.2 km, a latitude

of 34°.1, a maximum model altitude of 30 km, a distance between levels of 200 m, and a water vapor scale height of 2 km were used.

Decades of atmospheric monitoring and measurement show that these kinds of idealized atmospheres are never practically realized in the Earth's atmosphere, but their use can give good guidance on the gross behavior of the atmosphere, and in our case in the gross characteristics of any proposed WVR system.

Atmospheric emission model

The atmosphere is split into N layers, with layers presumed to extend halfway between the defined levels in the atmospheric model creation. Rays (lines of sight) are then traced through the atmospheric layers until they pass through the top of the defined atmosphere. The effective emission temperature is found by integrating the equation of transfer along the ray path. See Hase & Höpfner (1999) for a good description of this kind of atmospheric ray trace and some good references to historical literature on the subject.

Throughout this treatment, the Rayleigh–Jeans assumption is used, so that intensity B_ν is linearly proportional to the brightness temperature T_b. This will cause an error at higher frequencies, but is unimportant at the frequencies of interest for the VLA ($\nu \lesssim 50$ GHz).

The model uses 2-D cartesian coordinates x, and y, with the origin at the center of the Earth, and the observatory along the y-axis . A *ray* is defined as the set of points along a line:

$$\mathbf{r}(s) = \mathbf{a} + \mathbf{b}\, s \quad , \tag{8}$$

where $\mathbf{a}$ is the vector position of the starting point of the ray, $\mathbf{b}$ is a unit vector in the direction of the ray, and s is the distance along the ray. So, at the beginning of the ray trace we set $\mathbf{a_1} = (0, R_{Earth} + h)$, where h is the altitude of the observatory. The direction of the initial ray is set by the desired zenith angle (z): $\mathbf{b_1} = (\sin z, \cos z)$. The distance to the first boundary (s_1) is then calculated by performing a ray–sphere intersection test (see e.g., Haines 1989) with the sphere being defined by the radius of the upper boundary of the lowest atmospheric layer. The ray in the lowest layer is now all points along the ray with $s < s_1$. Appropriate quantities for that layer are then calculated (see below). The starting point of the ray in the next layer up (the 2^{nd} layer) is then defined by: $\mathbf{a_2} = \mathbf{a_1} + \mathbf{b_1}\, s_1$. To find the direction of the ray in the 2^{nd} layer, Snell's law is applied, using the ratio of the indeces of refraction in the 1^{st} and 2^{nd} layers. The method of Heckbert (1989) is used, noting that the incident ray (**I** in Heckbert) is $\mathbf{b_1}$, and the surface normal (**N** in Heckbert) is $-\mathbf{a_2}/|\mathbf{a_2}|$. This procedure is repeated up through the layers, yielding the ray parameters for each layer: $\mathbf{a}_i, \mathbf{b}_i$, and s_i for layer i. The ray trace is continued up through the layers until the ray has passed through the uppermost boundary in the atmospheric model.

The downwelling atmospheric brightness temperature is a sum of the contribution from

each atmospheric layer, attenuated by the opacity of all layers below it. This can be written:

$$T_{atm} = T_{CMB}\ e^{-\tau_{1,N}} + \sum_{i=1}^{N} T_i \left(1 - e^{-\tau_{i,i}}\right)\ e^{-\tau_{1,i-1}} \quad , \tag{9}$$

where T_i is the physical temperature of the i^{th} layer, $\tau_{b,c}$ is an opacity term, and T_{CMB} is the cosmic microwave background temperature, taken to be 2.7 K. The opacity term is:

$$\tau_{b,c} = \sum_{a=b}^{c} \tau'_a \quad . \tag{10}$$

The opacity of the i^{th} layer, τ'_i, is obtained by integrating along the ray in the layer ($\mathbf{r}_i(s) = \mathbf{a}_i + \mathbf{b}_i\, s$):

$$\tau'_i = \int_0^{s_i} k(s)\, ds \quad , \tag{11}$$

where $k(s)$ is the total atmospheric absorption at position s along the ray. This integral equation for the opacity in each layer could in principle be solved numerically, allowing for variation along the path through the layer (e.g., linear temperature and exponential pressure gradients), but in practice it makes little difference if the absorption is assumed constant throughout the layer, as long as the layers are thin enough. The absorption can be written (see e.g., Liebe 1985):

$$k = 0.042\ \nu\ N'' \quad , \tag{12}$$

where N'' is the imaginary part of the refractivity (the refractivity is $N = (n-1) \times 10^6$ for index of refraction n). The refractivity is calculated in each layer using the models of Liebe and coworkers (Liebe *et al.* 1993; Liebe 1989; Liebe 1985), with the possible modification of Rosenkranz (1998). These models also provide the real part of the refractivity, which is used in the calculation of the refraction between atmospheric boundary layers.

Figure 3 shows the derived brightness temperature at zenith as a function of frequency given the input model atmosphere described above and shown partially in Figure 2. Figure 4 focuses on the 18 - 26 GHz region of the spectrum, since this is the range for the upgrade K-band receivers, and hence of interest for this study.

Filters

Given the ability to calculate the atmospheric emission for a given atmospheric profile as a function of frequency, it is then relatively simple (though computationally more expensive) to do a numerical integration over frequency to simulate any given filter bandpass. In the current study I presume pillbox filters but arbitrary filter shapes are allowed for in the software.

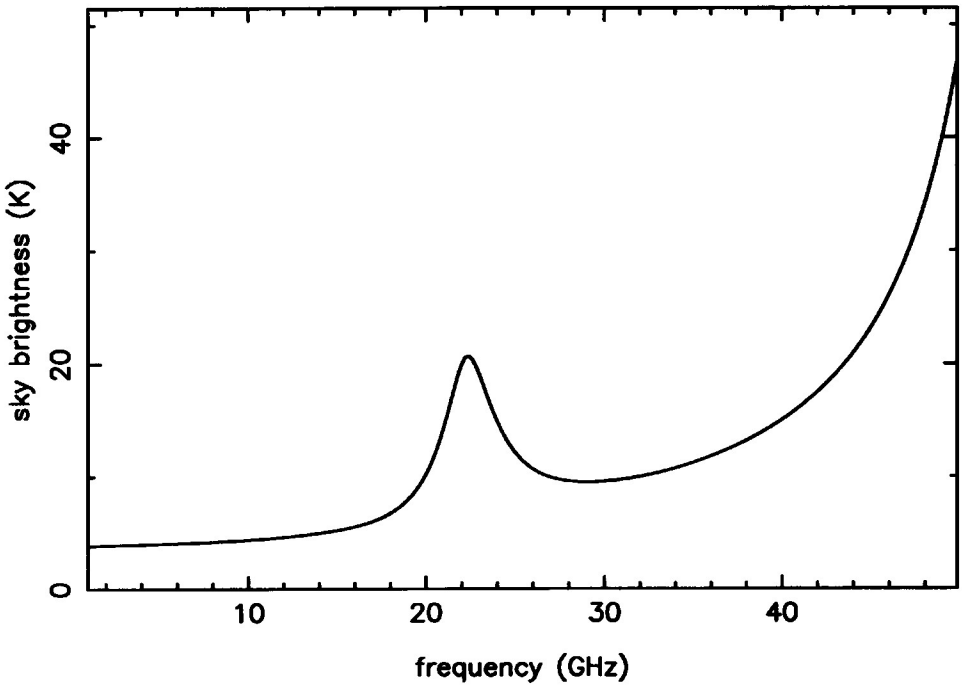

Figure 3: Sky emission as a function of frequency for the atmospheric model shown partially in figure 2.

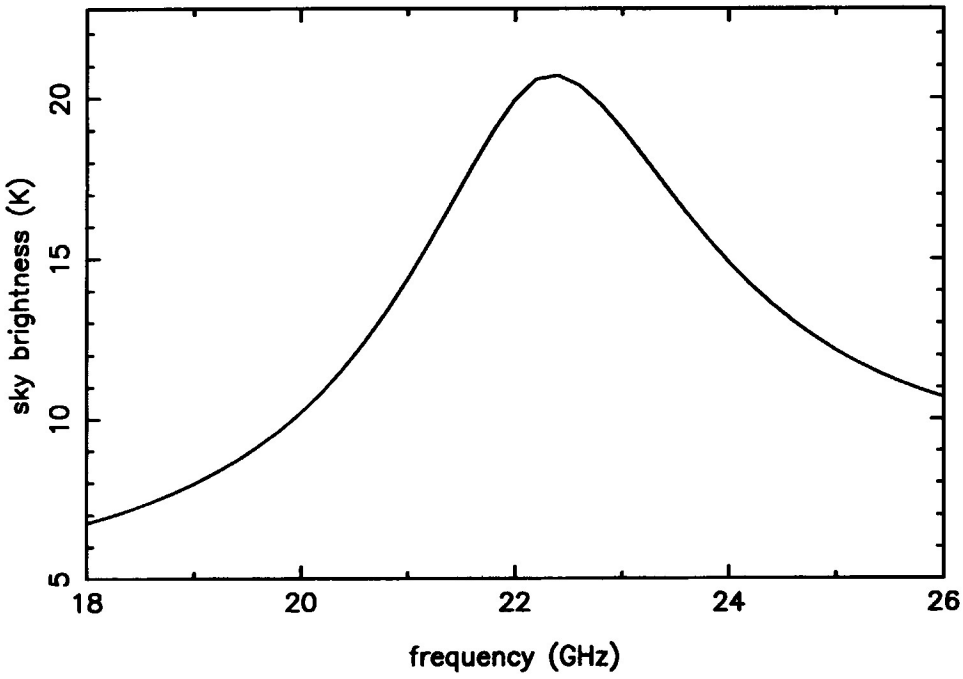

Figure 4: Same as figure 3 for frequencies in K-band.

Difference models

In order to simulate the effect of fluctuating water vapor along differential lines of sight for the antennas of an interferometer pair, I simply calculate the atmospheric emission (across a filter if desired) without and with some additional amount of water vapor. The details of the additional water vapor can be specified as the total amount (in precipitable microns), the width of the layer, and its altitude. In addition to additional water vapor in the path, I allow for temperature fluctuations in a layer. Finally, I allow for cloud to be considered above one antenna and not above the other. Given one (or any combination) of the above fluctuations, I then run the model many times with the specified fluctuations, but allowing either the total precipitable water vapor (PWV), the height of the fluctuations (h), the surface temperature (and hence the temperature throughout the atmosphere), or the water vapor scale height to vary in some specified range. I then gather statistics over those many runs. I can then compile statistics as a function of, for instance, the amount of fluctuating water vapor or temperature. This is similar to the technique of Staguhn *et al.* (1998), but they only ran one model for each desired set of parameters, rather than running many and gathering statistics.

Comparison of the Liebe models and some examples

How much difference does it make which of the Liebe models is used? Figure 5 shows a plot of a difference spectrum (at zenith) using the three different models of Liebe and coworkers - Liebe85, Liebe89, and Liebe93. This difference spectrum was created by taking the model atmosphere shown partially in Figure 2 and calculating an emission spectrum, then adding 35 μm of water vapor in a 20 m wide layer at 2 km altitude (above the surface) and calculating another emission spectrum, then taking the difference between these two spectra. Liebe85 and Liebe89 agree very well. Liebe93 is different, with a larger discrepancy between the two spectra. There has been some discussion of the believability of Liebe93 amongst atmospheric modelling groups, so I choose to use the Liebe89 model throughout the rest of this study.

Note that there are other models available (e.g., Rosenkranz 1998 or Cruz Pol *et al.* 1998). If we were concerned with absolute measurements of total atmospheric path (and its fluctuations), then it might become important to select the "best" (in some sense) of these available models. In fact, given that we are only interested in differential quantities here (the difference between two lines of sight that are only separated by a relatively small distance), I think it likely makes little difference which of the models is used.

Using the same atmospheric model as above, now take a temperature difference of 5 K in a 50 m layer at the same altitude. The resulting difference spectrum (again at zenith) is shown in Figure 6. It is easy to see that the additional water vapor has a much stronger signature than the additional temperature. Because of this, I do not treat temperature fluctuations further in this study.

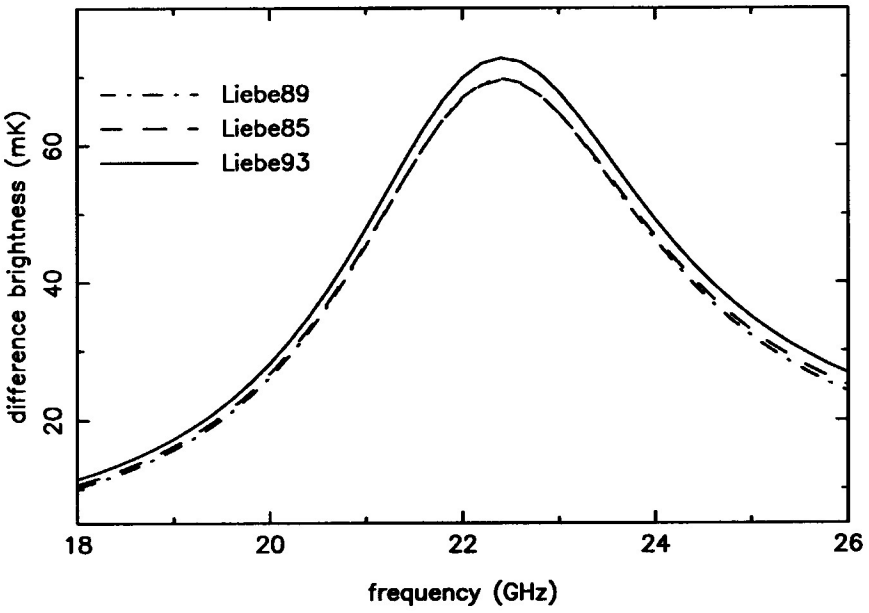

Figure 5: An example difference spectrum with additional water vapor in a layer.

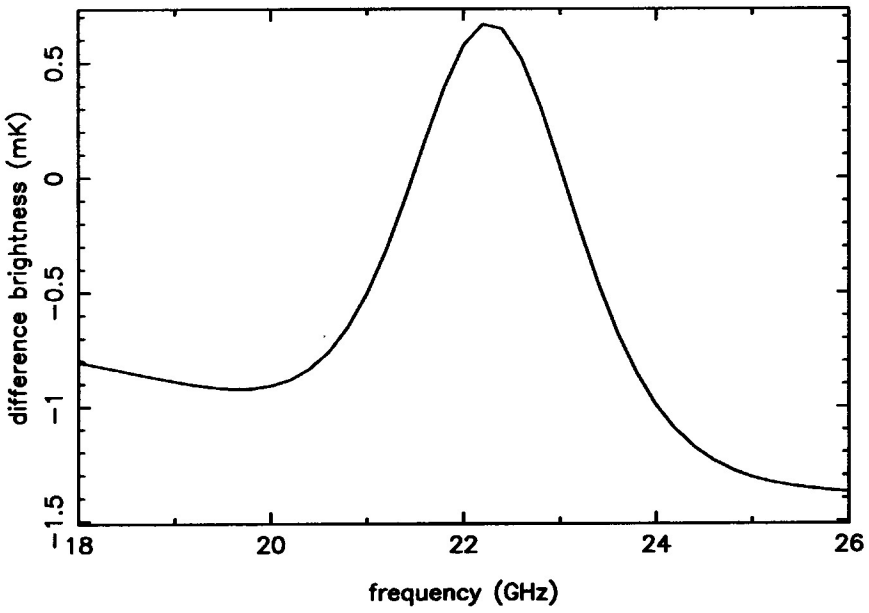

Figure 6: An example difference spectrum with additional temperature in a layer.

Filter selection

In this section, I will attempt to derive the required measurement sensitivity for a selection of filter numbers, widths and placements, and then discuss some implications. Some of the methodology in this section was inspired by Staguhn *et al.* (1998), who have done a somewhat similar study for the 22 GHz systems being developed for OVRO and BIMA. I do not intend to rigorously develop an optimized selection of channel number, width, and placement, since the parameter space is large and the computational cost is not trivial. I will rather concentrate on 4 current systems which are either already in existence, or are currently being developed. These 4 are: 1 - the current OVRO system; 2 - the originally designed VLA system (VLA_1); 3 - the current VLA system (VLA_2); and, 4 - the current ATCA design. Parameters for channel number, width, center frequency, and weight (defined below) are shown in Table 1. These are taken from Marvel & Woody (1998) for OVRO, and from the presentation of Bob Sault at the 1999 URSI meeting (Hall *et al.* 1999) for the ATCA. Note that I do not consider the many-channel case (as for the new correlating backend for OVRO/BIMA described in Staguhn *et al.*), but it is clear that it is superior in terms of ability to distinguish the fluctuations in water vapor. Figure 7 shows graphically

Table 1: Filter characteristics for the four study cases.

case	center frequency (GHz)	width (GHz)	weight
OVRO	19.2	2	-0.5
	22.2	2	+1.0
	25.2	2	-0.5
VLA_1	19.0	1	-0.5
	22.2	1	+1.0
	25.5	1	-0.5
VLA_2	21.0	0.35	-0.5
	22.2	0.5	+1.0
	23.5	0.35	-0.5
ATCA	16.0	1	+0.524
	18.4	1	-1.088
	23.0	1	+1.231
	25.0	1	-0.667

the information shown in Table 1 for the 4 study cases, along with the emission spectrum from Figure 4.

In each of these 4 cases, an "observable" can be defined as:

$$T_{obs} = \sum w_i \, T_i \quad , \tag{13}$$

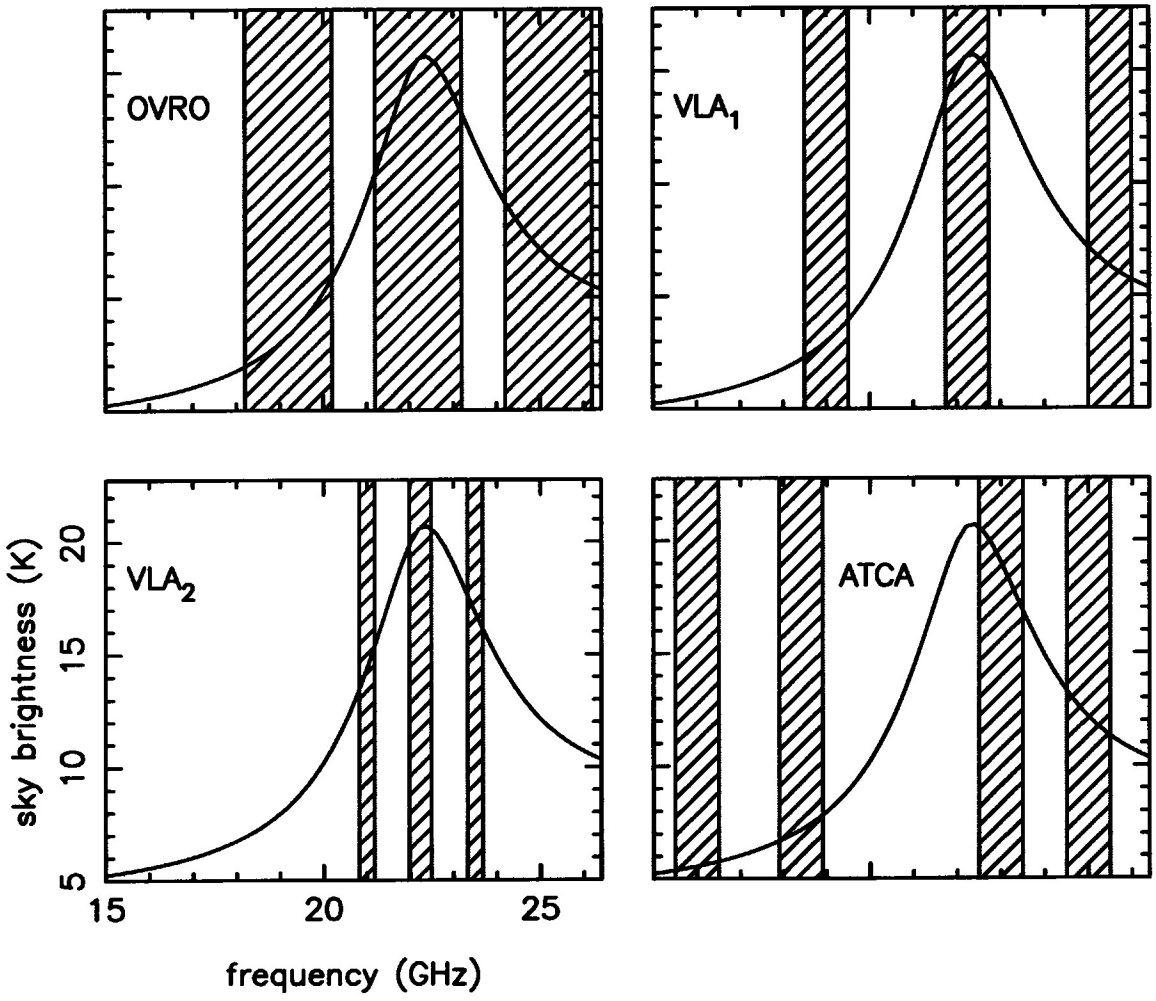

Figure 7: Graphic display of the filters for the 4 study cases.

where the w_i are weights (shown in Table 1), and the T_i are the measured atmospheric (or system) temperatures for the channels. This is the quantity which is considered to track line of sight water vapor (and hence interferometric phase) fluctuations. In the first 3 cases, the observable is a simple subtraction of the average of the two "wing" channels from the "line" channel. The ATCA case is more complicated, and in that case the weights were derived in an optimization.

In the following sections, I will show how the observable varies with the amount of additional water vapor using as input the simple atmosphere discussed above (in the Examples section) for each of the 4 cases. I will present results of model runs where the additional amount of water vapor is allowed to reach as much as 1 mm (this would be about 1 turn of phase at 7 mm). At each of a number of discrete values of additional water vapor, 500 model trials are done where in each trial, one or more of the parameters of interest are allowed to vary. These parameters are the height of the fluctuation, the total PWV, the surface temperature, and the water vapor scale height. The height of the fluctuation is allowed to vary from 0.5 to 3 km. The total PWV is allowed to vary from 0.5 to 12 mm. The surface temperature is allowed to vary from 0 to 20 C (this is about the range of mean monthly temperatures at the VLA). The scale height is allowed to vary from 1 to 3 km. In the following plots, the mean and 1-σ values of the observable are shown as a function of the additional water vapor. The number of 500 trials was chosen by examining how the 1-σ value varied as the number of trials was increased, and choosing a number where only about 1% of the variation was due to the number of trials (rather than the intrinsic variation from the variable parameter). Note that in the following, the zenith angle is 45 degrees in all cases.

Relative contributions of variations in parameters

Before presenting the observable and 1-σ value for each of the four cases when allowing all four of the parameters of interest to vary, I will first investigate the relative contribution from the variation of each of these four parameters of interest separately. In order to do this, I will present runs for the OVRO case where only 1 of the 4 parameters is allowed to vary. Figure 8 shows a plot of the observable against the amount of excess water vapor when each of the four parameters is allowed to vary separately. For the height of the fluctuating layer (varying from 0.5 to 3 km), at 35 μm of excess water vapor, the mean value of the observable is 53.4 mK, and its 1-σ value is 6.78 mK. For the total PWV (varying from 0.5 to 12 mm), at 35 μm of excess water vapor, the mean value of the observable is 56.4 mK, and its 1-σ value is 4.50 mK. For the surface temperature (varying from 0 to 20 K), at 35 μm of excess water vapor, the mean value of the observable is 56.7 mK, and its 1-σ value is 2.89 mK. For the scale height of the water vapor (varying from 1 to 3 km), at 35 μm of excess water vapor, the mean value of the observable is 55.7 mK, and its 1-σ value is 2.52 mK.

In some sense, the surface temperature here is a proxy for the ability to know the temperature distribution through the atmosphere, so it is hard to measure (in effect), but its

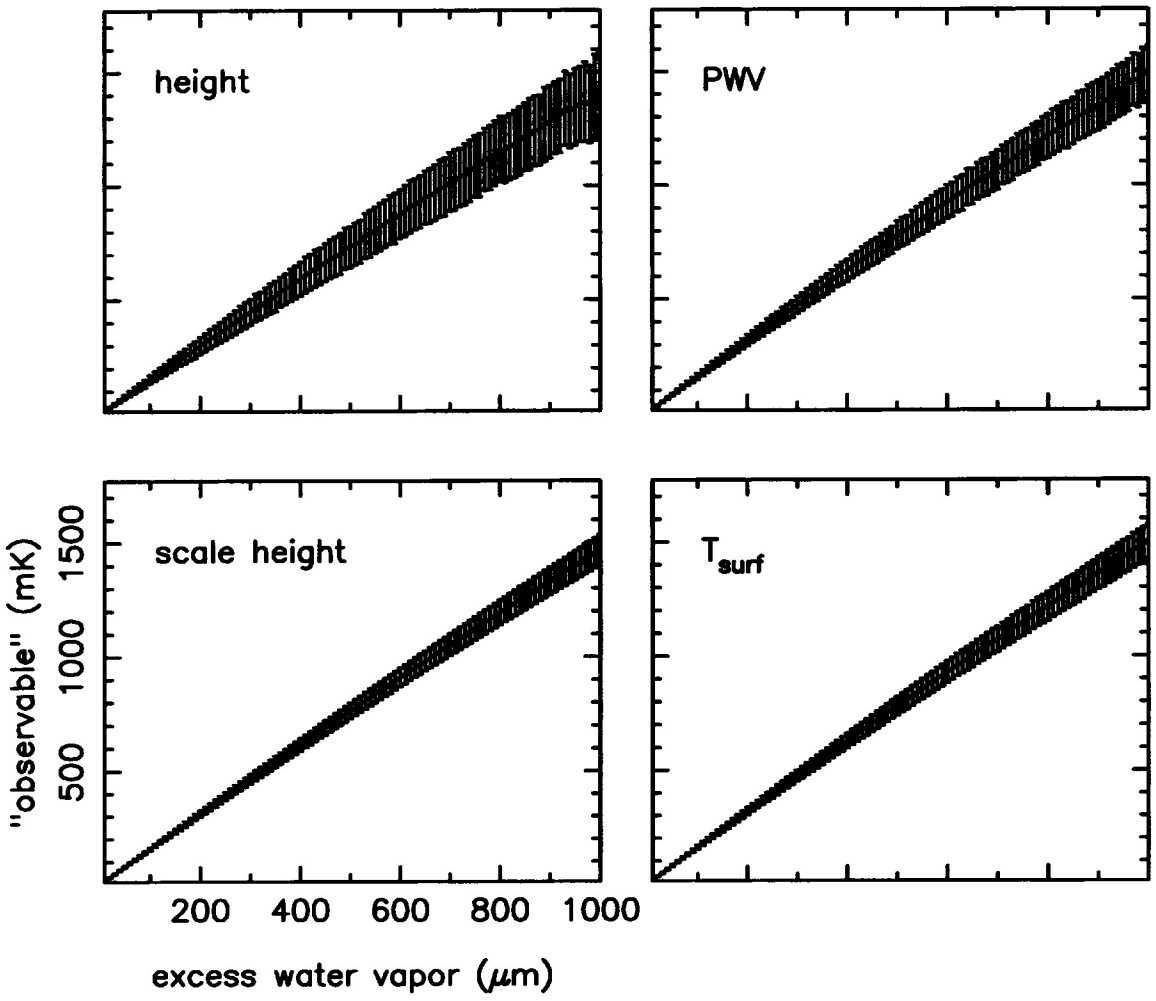

Figure 8: "Observable" for the OVRO example case allowing each of the four parameters of interest to vary separately.

fluctuation has a small effect on the variation in the observable. The water vapor scale height is also not easy to measure, but is actually not expected to deviate much from the 1.5-2 km range, and again only has a small effect on the variation of the observable. The total PWV has a larger effect on the variation of the observable, but can be estimated (at least crudely), given measurements of surface temperature and humidity (Butler 1998). The dominant parameter determining the variations in the observable is the fluctuation in the height of the excess water vapor layer. This is very unfortunate, as it is probably the hardest to measure (or estimate) of the 4 quantities. I will now present runs for each of the cases where all four of the parameters of interest are allowed to vary.

Allowing all 4 parameters to vary

Figure 9 shows a plot of the observable and 1-σ values against the amount of excess water vapor with added variations in all four of the parameters of interest for all 4 of the cases (filter sets). In the OVRO case, at 35 μm of excess water vapor the value of the observable is 55.5 mK and the 1-σ value is 7.7 mK. In the VLA_1 case, at 35 μm of excess water vapor the value of the observable is 65.0 mK and the 1-σ value is 9.4 mK. In the VLA_2 case, at 35 μm of excess water vapor the value of the observable is 25.5 mK and the 1-σ value is 6.0 mK. In the ATCA case, at 35 μm of excess water vapor the value of the observable is 65.3 mK and the 1-σ value is 8.8 mK.

Discussion

It seems from the results shown above that there is a nearly linear relation between the observable and the excess water vapor. If the values of excess water vapor are restricted to smaller values, this becomes even more evident. Figure 10 shows a plot of the observable for all 4 cases for values of the excess water vapor which result in less than 1 radian of phase fluctuation at 7 mm (about 180 μm of excess water vapor or 1.1 mm of total excess path). This linearity is, of course, one reason why such systems are able to successfully correct for phase fluctuations due to atmospheric water vapor. The best fit linear slope for the four cases is: OVRO - 1.573 mK/μm; VLA_1 - 1.831 mK/μm; VLA_2 - 0.726 mK/μm; and ATCA - 1.854 mK/μm. Figure 11 shows the result after subtracting this linear slope from the four cases, graphically illustrating the linearity of the result.

It is also evident from the treatment of the above 4 cases that the current VLA design is not necessarily a good one. It was thought that having the filters near the so-called "hinge points" (near the half-power points) of the line would make the system less susceptible to variations in the height of the fluctuating layer. In fact, although the 1-σ value goes down, the ratio of the expected value of the observable to that 1-σ value (which can be thought of as a kind of equivalent SNR) is worse than in the other 3 cases. In addition, the expected value of the observable is more than twice as small as in the other cases, meaning that the

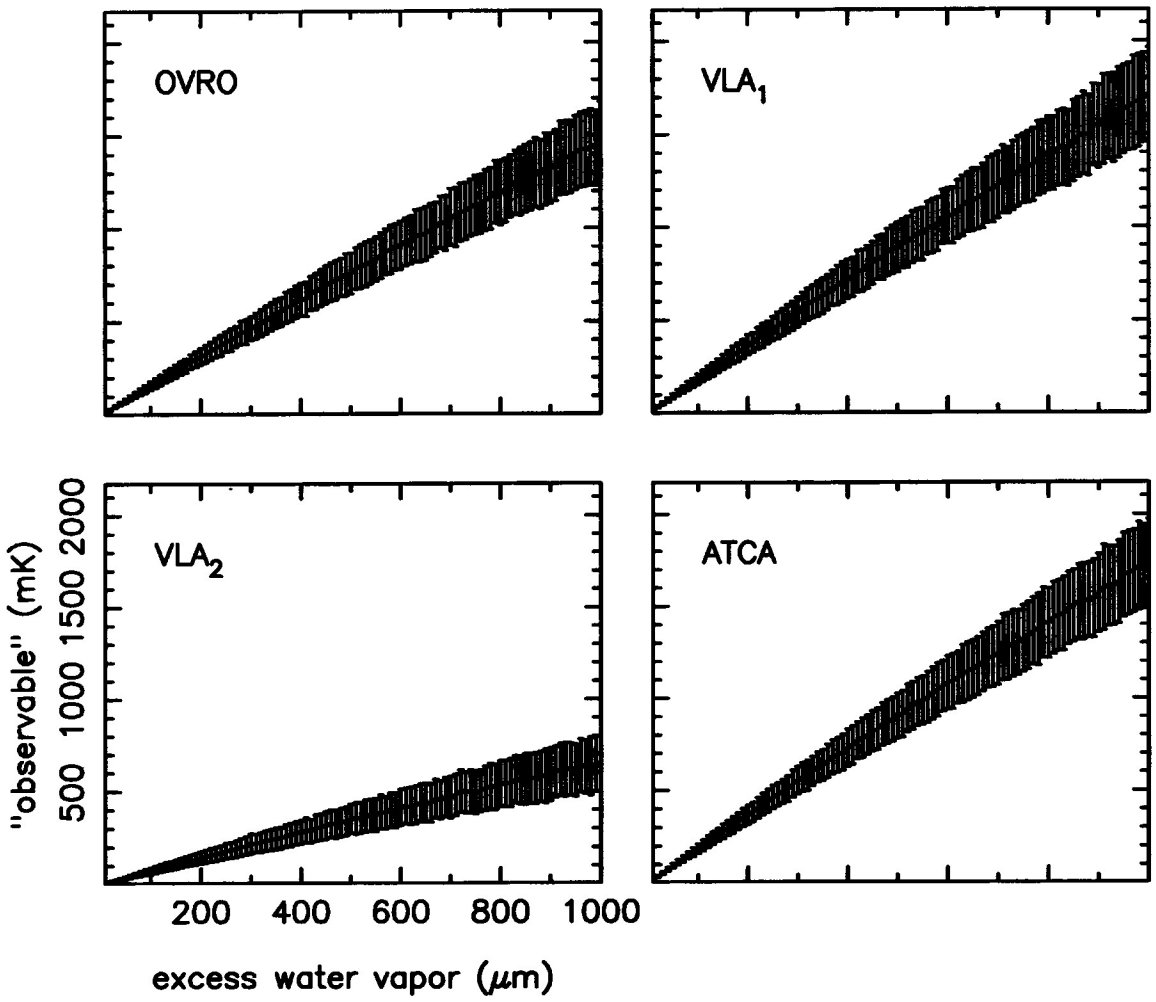

Figure 9: "Observable" for the four example cases with all four of the parameters of interest allowed to vary.

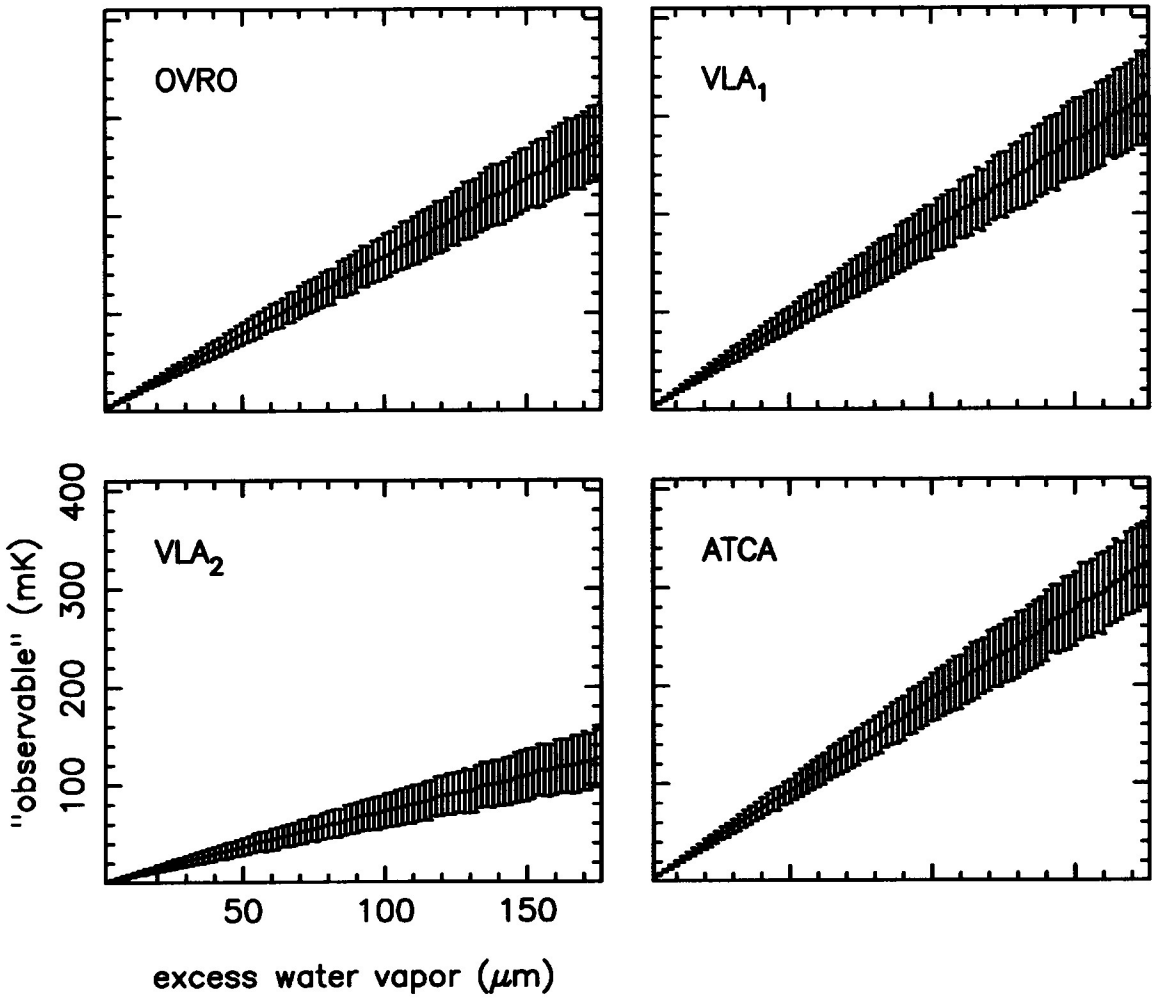

Figure 10: "Observable" for the 4 example cases for smaller amounts of excess water vapor.

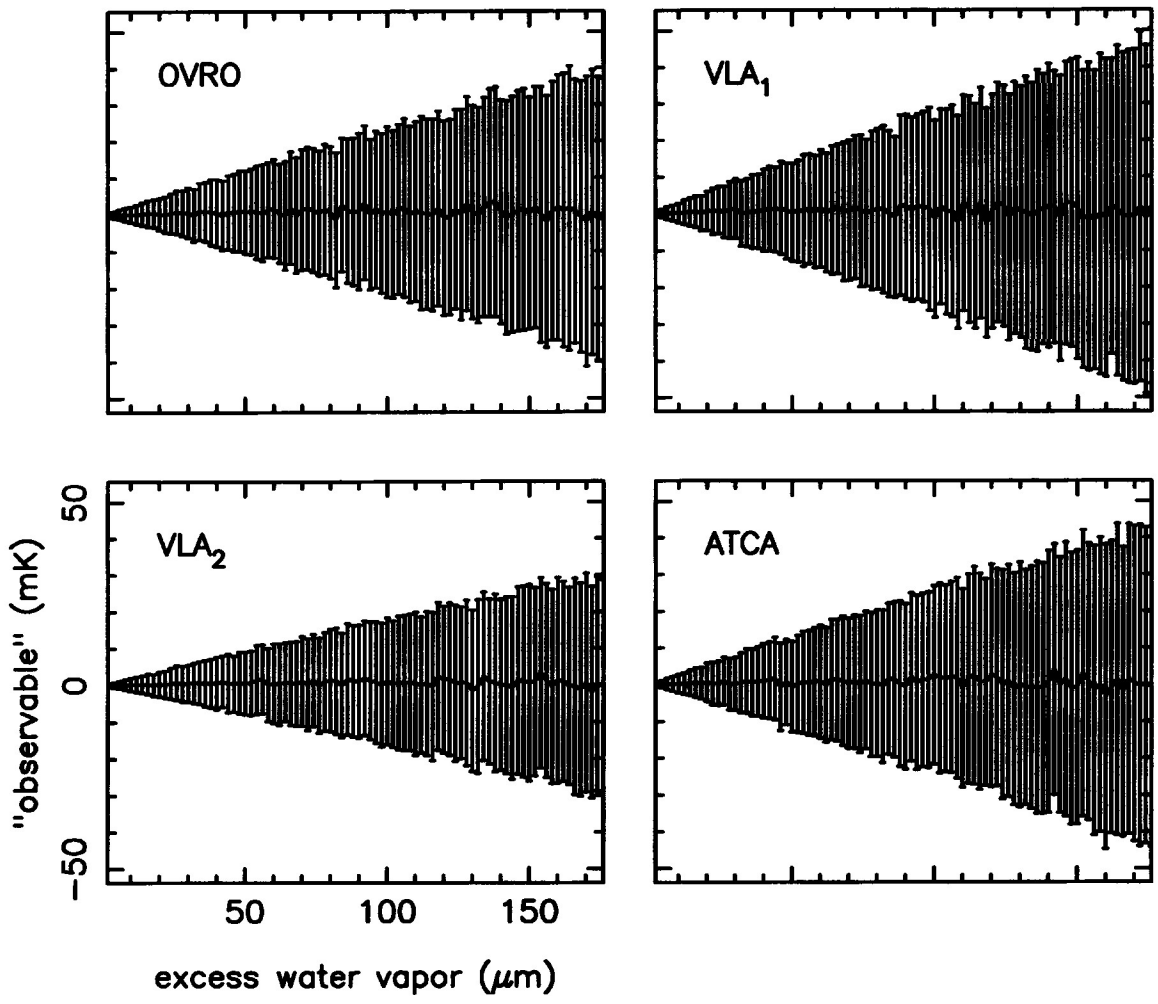

Figure 11: Residual in the "observable" for the 4 example cases for smaller amounts of excess water vapor after removal of a linear slope.

overall radiometry system sensitivity and stability needs to be better for this system. This makes the current filter locations and widths for the VLA design a nonoptimal choice. But, is it good enough? Table 2 shows the expected observable for the 4 cases at 35 μm of excess water vapor, the 1-σ variation with all of the fluctuations, and the expected sensitivity of the observable given by equation 4. The sensitivity was calculated assuming $\tau = 5/3$ s (this is 2 of the 5/6 second fundamental WVR data dump periods and is currently the shortest integration time commonly available for VLA observations), $T_{cal} = 5$ K, and $T_{sys} = 50$ & 100 K. Note that this calculation ignores gain and T_{cal} fluctuations, so is optimistic. It is clear that the goal is not reached under any conditions with the current WVR design. Even under the best conditions (when $\sigma_{T_{sys}} = 45$ mK), the detectable fluctuation is of order 60 μm of excess water, which corresponds to roughly 20° of phase at 7 mm. Note that the goal is met for the original VLA design, as long as T_{sys} is $\lesssim 75$ K (which is met if the opacity is roughly $\lesssim 13\%$).

Table 2: Summary for the four study cases.

case	observable at 35 μm excess water vapor (mK)	1-σ (mK)	$\sigma_{T_{sys}}$ (mK) $T_{sys} = 50$ K	$T_{sys} = 100$ K
OVRO	55.5	7.7	21.2	84.9
VLA_1	65.0	9.4	30.0	120
VLA_2	25.5	6.0	45.3	181
ATCA	65.3	8.8	45.3	181

What to do? Given that the current design does not meet the goal, there are several possible courses of action. Three somewhat obvious ones are: (1) relax the goal or simply admit that we will not meet it; (2) modify the design so that the goal is met; or (3) increase the integration time to increase the sensitivity.

Option (1) is unattractive, I think, and should be thought of only as a last resort.

Option (2) is preferable in some sense, but requires work on redesign. It might seem that the simplest fix would be to go back to the wider channels. Even given the problem of the LO leakage and the required 20.5-24 GHz filter, there is enough bandwidth to allow for 3 1 GHz channels. A possible filter configuration might then be 1 GHz filters centered at 21.0, 22.2, and 23.5 GHz. However, this is not a very good solution. Although the sensitivity of the radiometer is improved (equivalent to the VLA_1 case), the observable is essentially the same as the VLA_2 case, still below the sensitivity limit. So, with the requirement of the 20.5-24 GHz filter, there is no good solution via this option. How can we remove the need for that filter? Is it just better isolation in the 2-way splitter that is needed? Better isolation at the LO-injection point?

Option (3) might work, but we face the prospect of not correcting for phase fluctuations on short timescales. Given our knowledge of phase fluctuations on short timescales at the VLA from the site testing interferometer, we can expect about 1.8° of residual phase fluctuation (that left over after the WVR correction) at 7 mm if the correction is done at 5/3 sec (median conditions averaged over the day and year), 2.9° if done at 10/3 sec, 3.8° if done at 5 sec, and 6.0° if done at 10 sec (Butler & Desai 1999). These values increase to about 3.5°, 5.5°, 7.5°, and 12° for summer daytime median conditions. We can likely suffer the loss in going to 10/3 sec, but going to longer times will cause a deterioration in the effectiveness of the WVR correction in summertime or under conditions worse than the median. Unfortunately, increasing the integration time to 5/3 sec still does not bring the radiometer sensitivity to the level required to detect the observable with the current design ($\sigma_{T_{sys}} = 32.1$ and 128.3 mK for $T_{sys} = 50$ and 100 K). With 5 sec integrations and 50 K system temperature, the radiometer sensitivity just begins to become good enough to measure the observable. Note, however, that with the wider channel option discussed in the above paragraph and 5/3 sec integration time, the observable becomes detectable by the radiometer system under better conditions.

Clouds (liquid water)

Cloud emission model

In order to investigate concepts and orders of magnitude, consider a very simple cloud model where the cloud is the only emitter/absorber in the atmosphere, and it is a simple slab with constant properties. The emission in this case would be:

$$T_{Bcl} = T_{cl} \left(1 - e^{-\tau_{cl}}\right) \tag{14}$$

where T_{cl} is the physical temperature through the cloud and τ_{cl} is its opacity. This opacity can be estimated by (see e.g., Slobin 1982):

$$\tau_{cl} = 1.3 \times 10^{-3}\, \nu_{GHz}^2\, M_{cl}\, l_{cl}\, 10^{0.0122(291-T_{cl})-1} \quad , \tag{15}$$

where ν_{GHz} is the frequency in GHz, M_{cl} is the cloud liquid water content in g/m^3, and l_{cl} is the cloud thickness in km. Note the ν^2 dependence. For the simple case described above in the examples ($M_{cl} = 0.3$ g/m^3, $l_{cl} = 0.5$ km, and $T_{cl} = 270$ K), the above 2 equations reduce to: $T_{Bcl} \sim 9.4 \times 10^{-3}\ \nu_{GHz}^2$, which is of order 5 K near 20 GHz.

Now, the Liebe89 model has incorporated into it a liquid water opacity term, which should account for cloud. It is more complicated than the above simple expression for τ_{cl}, but in fact turns out to give similar results. Figure 12 shows a comparison of the contribution from our default cloud to the atmospheric emission in both the simple and Liebe89 cases, when incorporated into the full model. A layer width of 10 m in the cloud layer was used,

in order to well sample the cloud. Zenith angle was taken to be 0° for this simple example. Note the deviation from a ν^2 dependence now, which is caused by self-absorption in the cloud (it goes more like $\nu^{1.7}$ here). The difference between the simple Slobin model and the more complicated Liebe89 model is about 10%. I will use the Liebe89 model to stay consistent in this study.

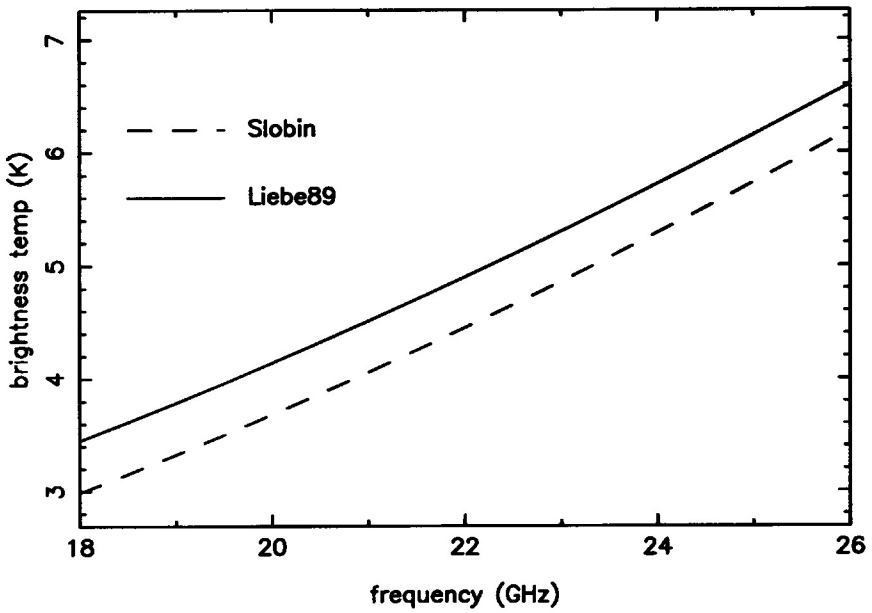

Figure 12: Comparison of cloud contribution for Slobin and Liebe89 cloud opacity models.

Cloud effect on WVR

Putting the cloud mentioned above into the atmospheric model (Liebe89), and calculating the observable for the 4 trial cases gives values of: -669.5 mK for OVRO; -632.9 mK for ATCA; -826.1 mK for VLA_1; and -502.3 mK for VLA_2. All of these values completely mask the real signal we are attempting to measure - that from excess water vapor.

It may be possible to design a new observable (by redefining the weights, e.g.) to be used when clouds are detected as being present, but that possibility is not investigated further here. Note, however, that the VLA_2 design, with the channels much closer to the line center, makes it harder to distinguish the presence of cloud.

Discussion

Further studies are needed in the area of cloud, particularly in the understanding of what types of cloud are present at the VLA site (e.g., water or ice, what liquid water content, height, extent, etc...), whether they modify the water vapor profile, and how or whether

WVR can possibly work in their presence. Currently it seems that the WVR may simply fail in their presence.

Beam divergence

Since in the current design, the WVR is intended to function at all times, there could be a problem when the subreflector is rotated to focus on a different receiver than the K-band receiver. In fact, in the current strawman feed ring layout for the VLA upgrade, the Ka-band and Ku-band receivers are nearly 180° away from the K-band receiver on the feed ring (see Figure 13). In all cases except when observing at K-band, the beam from the K-band feed

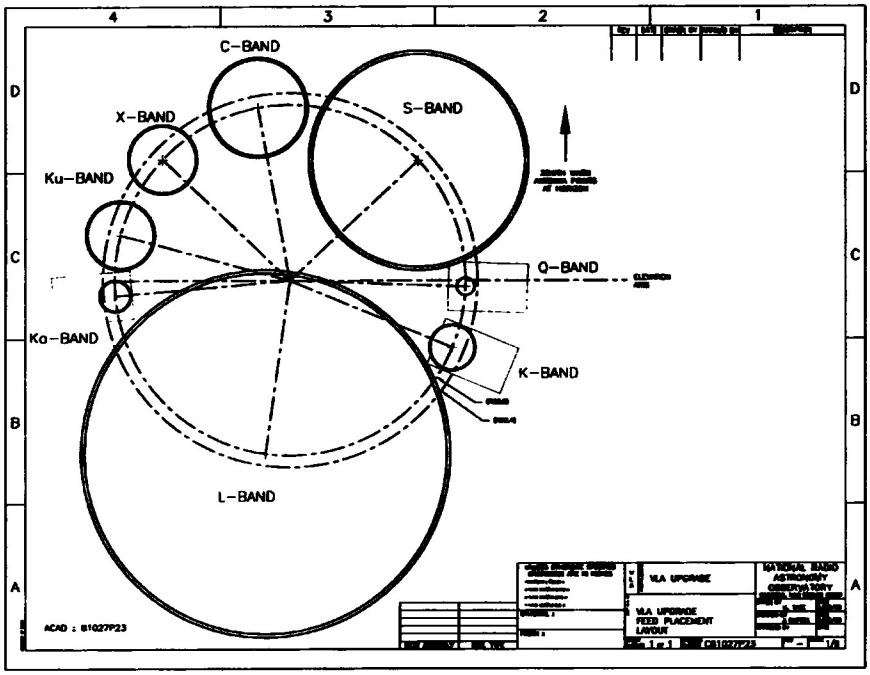

Figure 13: Strawman layout of receivers on the feed ring for the VLA upgrade.

will diverge from the astronomical beam. Figure 14 shows a cartoon illustration of this in the case when the astronomy feed is 180° from the K-band feed. In this case, the divergence angle θ can be approximated by:

$$\theta \sim \frac{D_{feed}}{M f} \quad , \tag{16}$$

where D_{feed} is the feed circle diameter (1.94 m), M is the magnification factor of the antennas (8.8), and f is the focal length of the antennas (9 m). Plugging in these numbers gives:

$$\theta \sim 1.4^\circ \quad . \tag{17}$$

At a height of 2 km, this is 50 m, or greater than the antenna main reflector diameter. Assuming that the wind speed in the turbulent layer is 10 m/s, this is like a 5 second lag,

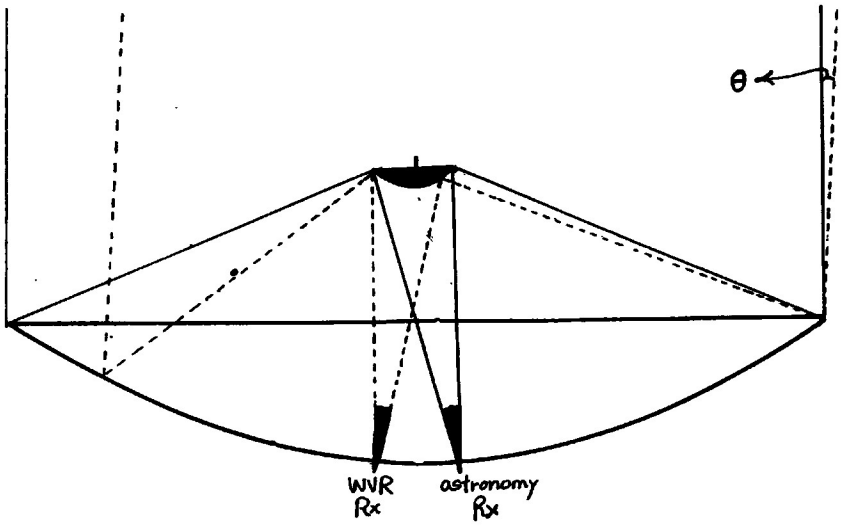

Figure 14: Illustration of beam divergence.

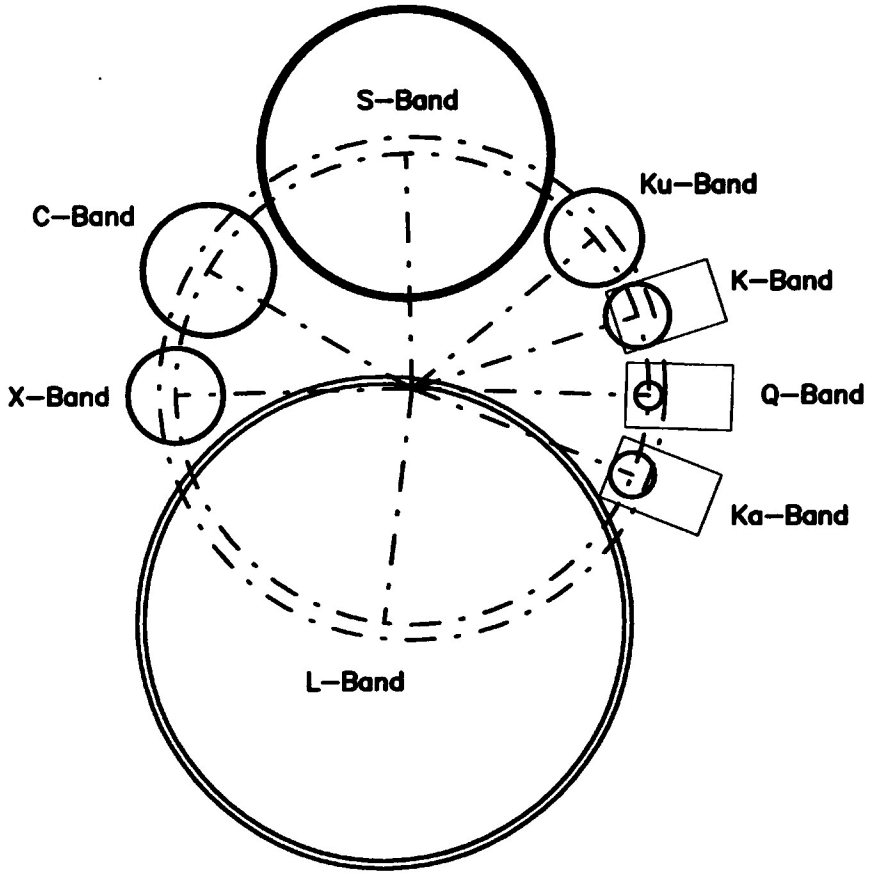

Figure 15: Possible revised layout of receivers on the feed ring for the VLA upgrade.

and, as discussed above, this results in unacceptably large residual phase errors. In order to overcome this problem, the high frequency feeds could all be placed near the K-band receiver on the feed ring (with all of them still as close to the elevation axis as possible, of course). Figure 15 shows one such possible layout, where the K-band feed has also been moved away from the L-band feed to reduce ground pickup (since this may be a problem for the WVR). In this layout, the high frequency feed furthest from the K-band feed is the Ka-band feed, with a separation of $\sim$ 65 cm. The beams from these two receivers will therefore diverge by only about 17 m, which is less than the antenna diameter, and should be acceptable.

Summary

- The goal for the VLA WVR system should be to measure water vapor fluctuations of 35 μm (total path length fluctuations of 220 μm).
- The current VLA design for the WVR will not meet this goal.
- The best solution to this problem seems to require a redesign of the electronics to get rid of the requirement of having the relatively narrow 20.5-24.0 GHz filter at the front end of the WVR.
- If that is not possible, at least we should go with the wider (1 GHz) channels (centered at 21.0, 22.2, and 23.5 GHz).
- We can probably get away with 5/3, and possibly with 10/3 sec integration times for the WVR data, but going to longer integrations will leave too much residual atmospheric phase fluctuation in many cases.
- Clouds are a problem, and will impair the ability to use any simple radiometry system to do WVR phase correction when they are present.
- We have a beam divergence problem with the upgrade feed ring layout. I've shown an alternate layout which might help ameliorate this problem.

Acknowledgements

The WVR system at the VLA would not exist without the expertise of Durga Bagri, Paul Lilie, and Galen Watts, who designed, built, and debugged most of the beast. Wayne Koski managed the monitor and control portion of the system, and Ken Sowinski managed the software portion. Kathy Tate was nice enough to dig up the feed ring illustration for me.

References

Bagri, D.S., A Proposal to Monitor T_{SYS} in New K-Band Frontends for Estimating Atmospheric Phase Variations, VLA Electronics Memo. No. 184, 1995

Bagri, D.S., Estimating Tropospheric Phase Variations for the VLA, VLA Test Memo. No. 184, 1994

Bastian, T.S., & A.H. Bridle, The VLA Development Plan, NRAO (see also http://www.nrao.edu/vla/html/Upgrade/Upgrade_home.shtml), 1994

Bremer, M., S. Guilloteau, & R. Lucas, Atmospheric Phase Correction Based on Sky Emission in the 210-248 GHz Band, in *Science with Large Millimeter Arrays*, ed. P. Shaver, Springer-Verlag, 1996

Buck, A., New Equations for Computing Vapor Pressure and Enhancement Factor, *J. Appl. Met., 20*, 1527-1532, 1981

Butler, B., Precipitable Water at the VLA – 1990-1998, VLA Scientific Memo. No. 176, 1998

Butler, B., & K. Desai, Phase Fluctuations at the VLA Derived From One Year of Site Testing Interferometer Data, VLA Test Memo. No. 222, 1999

Carilli, C.L., & M.A. Holdaway, Tropospheric phase calibration in millimeter interferometry, *Radio Sci., 34*, 817–840, 1999

Cruz Pol, S.L., C.S. Ruf, & S.J. Keihm, Improved 20- to 32-GHz atmospheric absorption model, *Radio Sci., 33*, 1319–1333, 1998

Haines, E., Essential Ray Tracing Algorithms, in *An Introduction to Ray Tracing*, ed. A. S. Glassner, Academic Press, New York, NY, 1989

Hall, P.J., R.J. Sault, & G.C. Carrad, Atmospheric Phase Correction for the Millimetre-Wave Australia Telescope, URSI General Assembly Abstracts, 841, 1999

Hase, F., & M. Höpfner, Atmospheric ray path modeling for radiative transfer algorithms, *Appl. Opt., 38*, 3129–3133, 1999

Heckbert, P. S., Writing a Ray Tracer, in *An Introduction to Ray Tracing*, ed. A. S. Glassner, Academic Press, New York, NY, 1989

Lay, O.P., M.C. Wiedner, J.E. Carlstrom, & R.E. Hills, CSO-JCMT Interferometer and 183-GHz radiometric phase correction, *Proc. SPIE, 3357*, 254-264, 1998

Lay, O.P., Phase calibration and water vapor radiometry for millimeter-wave arrays, *Astron. Astrophys. Suppl., 122*, 547–557, 1997

Liebe, H.J., G.A. Hufford, & M.G. Cotton, Propagation modeling of moist air and suspended water/ice particles at frequencies below 1000 GHz, AGARD (Advisory Group for Aerospace Research & Development) Conference Proceedings 542, 3-1–3-10, 1993

Liebe, H.J., MPM - an atmospheric millimeter-wave propagation model, International Journal of Infrared and Millimeter Waves, v.10, 631-650, 1989

Liebe, H.J., An updated model for millimeter wave propagation in moist air, Radio Science, v.20, 1069-1089, 1985

Marvel, K.B., & D.P. Woody, Phase correction at millimeter wavelengths using observations of water vapor at 22 GHz, *Proc. SPIE, 3357*, 442-452, 1998

Rosenkranz, P.W., Water vapor microwave continuum absorption: A comparison of measurements and models, Radio Science, v.33, 919-928, 1998

Slobin, S.D., Microwave noise temperature and attenuation of clouds: Statistics of these effects at various sites in the United States, Alaska, and Hawaii, *Radio Sci., 17*, 1443–1454, 1982

Sramek, R.A., Atmospheric phase stability at the VLA, VLA Test Memo. No. 175, 1989

Staguhn, J., A.I. Harris, R.L. Plambeck, & W.J. Welch, Phase correction for the BIMA array: atmospherical model calculations for the design of a prototype correlation radiometer, *Proc. SPIE, 3357*, 432-441, 1998

Sutton, E.C., & R.M. Hueckstaedt, Radiometric monitoring of atmospheric water vapor as it pertains to phase correction in millimeter interferometry, *Astron. Astrophys. Suppl., 119*, 559–567, 1996

Waters, J.W., Analysis of Water Vapor Data from the Greenbank Interferometer, NRAO Prog. Rep. 2, 1971

Waters, J.W., Atmospheric Effects on Radio Wave Phase and the Correction of Vapor-caused Phase Fluctuations by Radiometric Measurements of Water Vapor Emission, VLA Scientific Memo. No. 8, 1967

Watts, G., The Water Vapor Radiometer Section of the VLA 13mm (K-band) Receiver, NRAO electronics division internal report, May 1999

Welch, W.J., Correcting Atmospheric Phase Fluctuations by Means of Water-Vapor Radiometry, *Review of Radio Science 1996-1999*, ed. W.R. Stone, Oxford, 1999

Wiedner, M.C., Atmospheric Water Vapour and Astronomical Millimetre Interferometry, Ph.D. thesis, University of Cambridge, 1998

Wright, M.C.H., Atmospheric phase noise and aperture-synthesis imaging at millimeter wavelengths, *PASP, 108*, 520–534, 1996